

Effect of constitutive model parameters for FRC beams in different shear-span ratios

Y.Kaneko & H.Mihashi

Dept. of Architecture & Building Science, Tohoku University, Sendai, Japan

ABSTRACT: The objective of this paper is to examine the performance of constitutive models for describing the cracking behavior and the load-displacement characteristics of shear failure of concrete structures. Fiber reinforced concrete beams in different shear-span ratios (0.3 to 4.0) were analyzed. The structural analysis was carried out by means of the nonlinear finite element method. A smeared crack approach using a rotating crack model without shear strain on the crack plane was employed. Based on this analytical work, the effect of the softening parameters in constitutive laws for shear behavior of concrete beams in different shear-span ratios was discussed. Furthermore, the sensitivity of numerical results to the web reinforcement was investigated.

1 INTRODUCTION

The mechanism of shear fracture in concrete structures has been the subject of heated debate in past decades. Yet, it has not been sufficiently clarified. On the other hand, several crack approaches as well as constitutive models for concrete have been proposed by many researchers (e.g. Hordijk et al. 1989). However, reliable predictions for the extreme complex shear failure in concrete structures have not been achieved. The complexity of the shear failure depends considerably on how much the failure mode is governed by the crushing of concrete.

There are two representative numerical approaches for implementing a crack model based on fracture mechanics: the discrete crack approach and the smeared crack approach (e.g., Hillerborg and Rots 1989). The discrete crack approach is a direct application of crack models. Crack growth is analyzed on the assumption that cohesive forces are acting in the process zone. If the crack path is not known in advance, the problem is complicated. In the smeared crack approach, a cracked solid is assumed to be a continuum with the notion of stress and strain (Rots & Blaauwendraad 1989). The behavior of cracked concrete can then be described in terms of stress-strain relations and it is sufficient to switch from the initial isotropic stress-strain relation to an orthotropic stress-strain relation upon cracking. In such a way, the topology of the original finite element mesh remains preserved which is computationally convenient. The two approaches seem to achieve better performance in different types of ap-

plications. In general, the smeared approach is better suited for engineering analyses of distributed fracture, while the discrete approach has its strength in detailed analyses of localized fracture. Thus, the smeared crack approach may be employed for a rough estimation of the load-displacement relation of shear failure of concrete structures in the practical design.

In this study, FRC (Fiber Reinforced Concrete) deep beam tests with web reinforcement (Mansur & Ong 1991) were numerically simulated in practice. In addition, in order to expand the comprehension on the effect of constitutive model parameters in the deep beams to slender beams, the beam in the shear-span ratio of 4.0 was numerically analyzed. Numerical simulations were carried out in a two-step procedure to examine the performance of constitutive models on describing cracking behavior and load-displacement characteristics of shear failure of concrete structures. First, the appropriate parameters are determined in both compressive and tensile constitutive models so as to approximate the peak load and load-displacement relation obtained in the experiments, and to describe the cracking behavior observed in the experiments. This analysis is considered as the benchmark analysis. Thereafter, the sensitivity of the numerical results to the compression and tension softening parameters is examined. This analysis is considered as the parametric analysis. Based on this analytical work, the effect of the softening parameters in the constitutive laws on shear behavior of concrete beams in different shear-span ratios is investigated.

2 BENCHMARK ANALYSIS

2.1 Deep Beam and Slender Beam

The specimens and loading system for the FRC deep beam tests (Mansur & Ong 1991) are shown in Figure 1. The beams with the minimum and the maximum shear-span ratio are analyzed in this paper, calculating the shear-span ratio $a/d = 0.3$ for Beam B1 and $a/d = 1.9$ for Beam B5. The beams were provided with four 16-mm diameter deformed main steel bars (yield strength $f_y = 440$ MPa) placed in two layers at the bottom, and these steel bars were welded to a 15-mm thick steel plate at each end. The web reinforcement comprised 6-mm diameter mild steel bars ($f_y = 375$ MPa). The ratio of the longitudinal and transverse web reinforcement was $\rho_l = 0.50\%$ and $\rho_t = 0.44\%$, respectively. Steel fibers were straight but slightly twisted, and were 30-mm long and 0.5-mm square in cross section. The fiber volume fraction was 1.0%. For the concrete, a water-cement ratio of 60% and the maximum aggregate size of 10 mm were adopted. The compressive strength f_c of FRC is 35.7 MPa for Beam B1 and 31.5 MPa for Beam B5.

The shear tests were conducted in a displacement-control-testing machine. The deflection in the center of the beam was measured by a linear variable differential transformer. In the experiment, the following cracking behavior was observed (Mansur & Ong 1991): The diagonal cracks within the shear span were the first to form. These cracks appeared approximately at mid-depth of the beam and propagated towards both the supporting and loading points. Further increase in load resulted in the propagation and widening of the existing cracks. Simultaneously, new diagonal cracks have developed more or less parallel to the existing ones. In the case of Beam B5, one of the diagonal cracks began to grow excessively wide, finally leading to failure. At impending failure, some crushing of the concrete was observed between the loading points and the tip of the major inclined crack. In the case of Beam B1, final failure occurred by crushing of the concrete in between the diagonal cracks.

Slender Beam considered here is identical to Beam B5 except the shear-span ratio and the amount of the main steel bar. The shear-span ratio of Slender

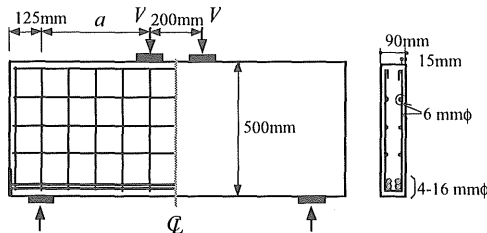


Figure 1. Specimens and Loading System.

Beam is assumed $a/d = 4.0$, and the amount of the main steel bar is reduced to 25% (one 16-mm diameter deformed steel bar, $f_y = 440$ MPa). Therefore, Slender Beam is expected to have a flexural failure.

2.2 Finite Element Analysis

The numerical simulations were carried out using SBETA (1997) Finite Element Program developed by V. Cervenka et al. A smeared crack approach using a rotating crack model was employed. In addition, the following effects of concrete behavior were considered: nonlinear behavior in compression including hardening and softening; fracture of concrete in tension based on nonlinear fracture mechanics; biaxial stress failure criterion according to Kupfer (1969) by means of equivalent uniaxial stress-strain relationship (Chen et al. 1982); reduction of compressive strength after cracking (Kollegger et al. 1988). The details of numerical formulation are given in SBETA (1997).

The present numerical study focuses mainly on the softening parameters of the constitutive models. Regarding the compressive constitutive models, the reduction of the compressive strength after cracking in the direction parallel to the cracks was applied, and several strength reduction rates were considered. A linearly descending softening law in compression was adopted and the influence of the end-point of the softening curve on the predicted load-deflection relations was also examined. Regarding the tensile constitutive models, a bilinear crack opening model and a tension cut-off model were alternatively employed. In the rotating crack model (Vecchio & Collins 1986), the direction of the principal stress coincides with the direction of the principal strain. No shear strain occurs on the crack plane and only two normal stress components must be defined. If the principal strain axes rotate during loading, the direction of cracks also rotates.

The behavior of concrete in tension without cracks was assumed to be linear-elastic. After cracking, two types of models were alternatively used in this analysis for the crack opening: a bilinear model (see Fig. 2a) and a tension cut-off model (see Fig. 2b) which has no softening regime and an abrupt stress-drop after cracking. The bilinear model was used with the following post-tensile strength f_{tc} based on the work of Lim et al. (1986):

$$\sigma_t = E_0 \varepsilon_t \quad (\varepsilon_t \leq \varepsilon_{cr}) \quad (1a)$$

$$\sigma_t = \alpha f_t^{ef} \quad (\varepsilon_t > \varepsilon_{cr}) \quad (1b)$$

$$f_{tc} = 2\eta_l \eta_0 \tau_{uf} V_f \frac{l_f}{\phi_f}, \quad \alpha = \frac{f_{tc}}{f_t}, \quad \varepsilon_{cr} = \frac{f_t^{ef}}{E_0} \quad (1cde)$$

where σ_t is the normal stress in the crack; E_0 is the initial elastic modulus; ε_t is the tensile strain; f_t^{ef} is the effective tensile strength associated with the

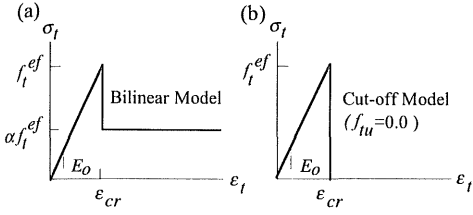


Figure 2. Constitutive Model in Tension.

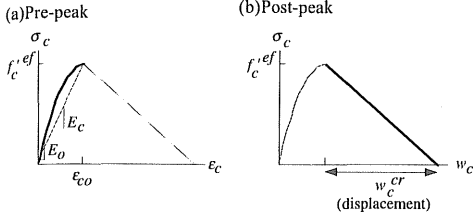


Figure 3. Constitutive Model in Compression.

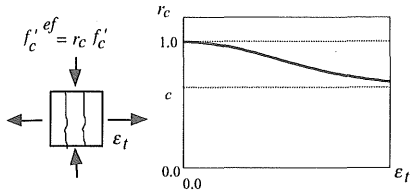


Figure 4. Compressive Strength Reduction Rate.

biaxial stress failure criterion according to Kupfer (1969); η_l is the length efficiency factor for fiber; η_o is the fiber orientation factor; τ_{uf} is the ultimate bond strength of fiber; V_f is the fiber volume fraction; l_f is the fiber length; ϕ_f is the equivalent fiber diameter; and f_t is the uniaxial tensile strength of FRC. The values of η_b , η_o and τ_{uf} are assumed 0.5, 0.33 and 4.12 MPa, respectively as suggested by Mansur & Ong (1991).

For the ascending branch of concrete stress-strain curve in compression, the formula recommended by CEB-FIP Model Code 90 (1990) was adopted (see Fig. 3a).

$$\sigma_c = f_c^{ef} \frac{kx - x^2}{1 + (k-2)x}, \quad x = \frac{\epsilon_c}{\epsilon_{c0}}, \quad k = \frac{E_0}{E_c} \quad (2)$$

where ϵ_c is the compressive strain; σ_c is the compressive stress; f_c^{ef} is the effective compressive strength associated with the biaxial stress failure criterion according to Kupfer (1969); ϵ_{c0} is the strain at the peak stress; k is a shape parameter and the value of 2.0 is used in this analysis for parabola; E_0 is the initial elastic modulus; and E_c is the secant elastic modulus at the peak stress.

For the descending branch of concrete constitutive curve in compression, a fictitious compression plane model is used based on the assumption that a compression failure is localized in a plane normal to the direction of principal compressive stress. All post-peak compressive displacements and energy dissipation are localized in this plane, and the post-peak compressive displacement w_c is derived from compressive strains based on the same concept as the crack band theory (Bazant & Oh 1983). The failure bandwidth is defined as the projection of the finite element dimension on the failure plane, and the direction of the failure plane is assumed to be normal to the principal compressive stress. It is assumed that the displacements are independent on the size of the structure and such hypothesis is supported by experiments conducted by van Mier (1986). Softening law in compression is linearly descending. The end point of the softening curve is defined as a limit displacement w_c^{cr} at the complete release of stress (see Fig. 3b).

The reduction of the compressive strength after cracking in the direction parallel to cracks is considered in a similar way as found in the experiments of Vecchio & Collins (1986). The reduction function was empirically developed by Kolleger et al. (1988) as follows:

$$f_c^{ef} = r_c f_c', \quad r_c = c + (1-c)e^{-(128\epsilon_t)^2} \quad (3)$$

where r_c is the compressive strength reduction rate; ϵ_t is the transverse strain (crack opening strain); and f_c' is the uniaxial compressive strength of FRC. For zero transverse strain, there is no strength reduction and for large strains the strength asymptotically approaches to the minimum value $f_c^{ef} = cf_c'$ (see Fig. 4). The constant c is the maximum strength reduction rate under a large transverse strain.

In the constitutive models, the initial elastic modulus E_0 and the uniaxial tensile strength f_t of FRC are estimated from the following equations (ACI 1989, Chen 1982):

$$E_0 = 4733\sqrt{f_c'} \quad (MPa) \quad (4)$$

$$f_t = 0.332\sqrt{f_c'} \quad (MPa) \quad (5)$$

2.3 Comparison and Discussion

The FEM model employed here was chosen to describe the test configuration of Mansur & Ong (1991). The FEM model for Beam B5 is shown in Figure 5. Considering the symmetry of the specimen, only half of the structure is analyzed. It should be noted that the strength of the hatched elements in the figure is increased by 80% to consider the three dimensional compression state due to the restraint of the bearing plates. The specimen is assumed to be in

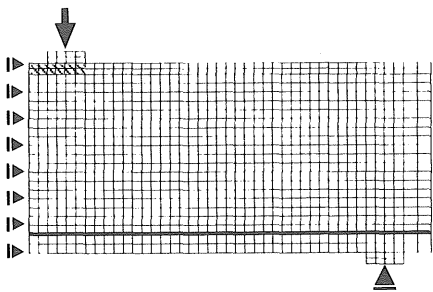


Figure 5. Configuration of FEM Model for Beam B5.

a state of plane stress. Finite plane stress elements consist of quadrilaterals. The stress-strain relation of reinforcement is assumed as perfectly elasto-plastic. The main steel bar (thick line) at the bottom of the beam is modeled by a discrete bar finite element, which is embedded and passing through quadrilateral elements as shown in Figure 5. The bar element has only axial stiffness and is in the uniaxial stress-state. It should be noted that on a macro-level, a relative slip distance of reinforcement with respect to concrete over a certain distance arise, if concrete is cracked or crushed. The longitudinal and transverse web reinforcement is modeled by a smeared reinforcement which stress and stiffness are considered in the quadrilateral element. While the vertical displacement of the support of the specimen is restrained, a vertical prescribed displacement is applied at the loading point. In the benchmark analysis, a bilinear model in tension (see Fig. 2a) and the limit displacement $w_c^{cr} = 2.0$ mm in compression

(see Fig. 3b) are adopted. To approximate the peak load, $c = 0.0$ was assumed for Beam B1 ($a/d = 0.3$), and no strength reduction ($c = 1.0$) for Beam B5 ($a/d = 1.9$) and Slender Beam ($a/d = 4.0$).

First, the cracking behavior predicted by the FEM analysis is examined. The cracking patterns at the peak load for Beams B1, B5 and Slender Beam are shown in Figure 6. In the figures, the hatched area indicates the crushed concrete, and the thicker crack line indicates the larger crack width. In the case of Beam B1, flexural cracks initiate at the bottom of the beam and subsequently diagonal cracks initiate at the web concrete. At the load level close to the peak, heavy crushed concrete areas associated with widely-opened diagonal cracks (crushing of concrete strut between diagonal cracks) near the upper and lower bearing plates grow abruptly, leading to a final failure.

In the case of Beam B5, flexural cracks initiate at the bottom of the beam and propagate to the mid-depth of the beam. Subsequently, diagonal cracks initiate at the web concrete and continue to propagate along the line between the loading point and the support, and grow excessively wide. Nearly at the peak load level, the compression failure is observed at the extreme compression fiber, leading to a final failure. Based on these comparisons, it may be concluded that the FEM model in the benchmark analysis for deep beams captures overall the cracking and crushing behavior associated with the shear-span ratio observed in the experiment.

In the case of Slender Beam, flexural cracks initiate at the bottom of the beam and propagate to the mid-depth of the beam. Subsequently diagonal

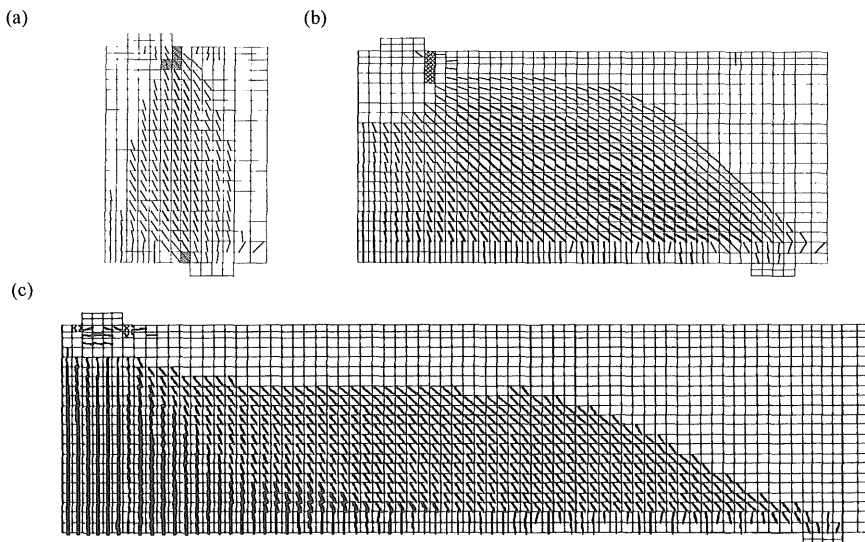


Figure 6. Cracking Patterns at Peak Load (a) Beam B1 (b) Beam B5 (c) Slender Beam.

cracks initiate at the web concrete and continue to propagate in a diagonal direction. At the load level close to the peak, the flexural cracks propagate to the upper-depth of the beam, and grow excessively wide, accompanied with the compression failure at the extreme compressive fiber. The failure load is associated with the yield of the main reinforcement.

Figure 7 shows a comparison between the results of load-deflection (in the center of the beam) relations in the experiment and in the FEM analysis. It should be noted that the predicted load-deflection curve for Beam B1 still gives relatively large peak load though the maximum compressive strength reduction rate $c = 0.0$ was used. This may indicate that further compressive strength reduction after cracking is necessary in this case. The numerical simulation captures the load-displacement characteristics with allowable deviation in the engineering analysis. Based on the examination of both the cracking behavior and the load-displacement characteristics, the current FEM model is used as the benchmark analysis to examine the effect of constitutive model parameters.

3 PARAMETRIC ANALYSIS

3.1 Influence of Softening Parameters

Figure 8 shows the comparison between the results of load-deflection relations in the benchmark analysis and in the parametric analysis with the maximum strength reduction rate c of 0.0 or 1.0. In the parametric analysis, the tensile constitutive model and the quantity of w_c^{cr} are identical to those in the benchmark analysis. There is somewhat difference of the peak load between $c = 0.0$ and $c = 1.0$ in

Beam B1, and little difference in Beam B5. This may be considered that the web reinforcement considerably reduces the sensitivity of the numerical results to the compressive strength reduction rate. Specifically, the longitudinal web reinforcement restrains the crack opening in the shear-span ratio $a/d = 0.3$ (Beam B1), and the transverse web reinforcement restrains it in the shear-span ratio $a/d = 1.9$ (Beam B5).

Figure 9 shows the comparison between the results of load-deflection relations in the benchmark analysis and in the parametric analysis with the limit displacement $w_c^{cr} = 1.0$ mm (half of the values in the benchmark analysis). In the parametric analysis, the tensile constitutive model and the quantity of c are identical to those in the benchmark analysis. The limit displacement w_c^{cr} considerably influences the entire load-displacement relation as well as the peak load in the shear-span ratio $a/d = 1.9$ (Beam B5). The larger limit displacement leads to a higher peak load. However, in the shear-span ratio $a/d = 0.3$ (Beam B1), this parameter does not influence the entire load-displacement relation as well as the peak load. This may be explained by the fact that in the case of $a/d = 0.3$, the abrupt load drop after the peak load is associated with the crushed concrete zone, which rapidly distributed along the shear plane. The stress redistribution is therefore not allowed. In the case of $a/d = 1.9$, the large limit displacement allows the stress to be redistributed, resulting in the increase of the peak load. Thus, the post-peak ductility in the compressive constitutive model allows the increase of the load-carrying capability of concrete beams in the case of $a/d = 1.9$.

Figure 10 shows the comparison between the results of load-deflection relations in the benchmark

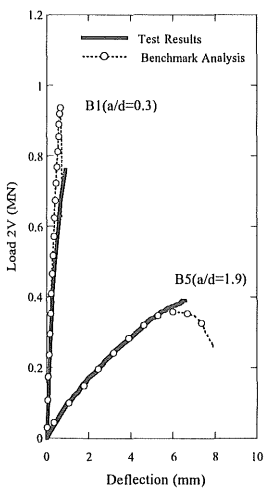


Figure 7. Comparison between Experiment and Benchmark Analysis.

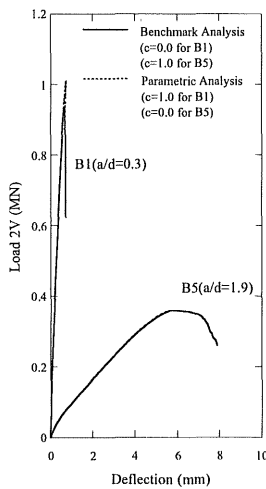


Figure 8. Comparison with Parametric Analysis in terms of c .

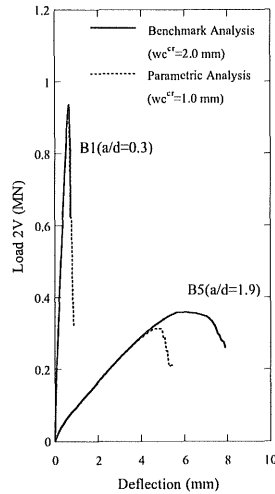


Figure 9. Comparison with Parametric Analysis in terms of w_c^{cr} .

analysis and in the parametric analysis with the tension cut-off model ($f_{tu} = 0.0$). In the parametric analysis, the quantities of the maximum strength reduction rate c and the limit displacement w_c^{cr} are identical to those in the benchmark analysis. There is no obvious difference in the numerical results for the case of $a/d = 0.3$ (Beam B1). However, the tension cut-off model gives a relatively low load-carrying capability in the case of $a/d = 1.9$ (Beam B5). Thus, the post-peak ductility in the tensile constitutive model allows the increase of the load-carrying capability of concrete beams in the case of $a/d = 1.9$.

Figure 11 shows the comparison of Slender Beam between the results of load-deflection relations in the benchmark analysis and in three parametric analyses with c of 0.0, $w_c^{cr} = 1.0$ mm and $f_{tu} = 0.0$, respectively. The numerical results are sensitive to the quantity of neither c nor w_c^{cr} . This may be explained by the fact that the failure mode of Slender Beam is the flexural failure associated with the yield of the main reinforcement, and therefore c and w_c^{cr} do not influence the numerical results. Thus, there is little effect of compressive softening parameters for the beams if the flexural failure mode is dominant. However, the post-peak ductility in the tensile constitutive model allows the significant increase of the load-carrying capability of concrete beams in the case of $a/d = 4.0$.

3.2 Influence of Web Reinforcement

In the previous section, it was qualitatively discussed that the web reinforcement reduces the effect of constitutive model parameters. To examine the influence of the web reinforcement further, the pa-

rametric analysis is carried out by removing the longitudinal or the transverse web reinforcement for Beam B1 ($a/d = 0.3$) and Beam B5 ($a/d = 1.9$).

Figures 12 and 13 show the comparison between the results of load-deflection relations in the benchmark analysis and in the parametric analysis without longitudinal web reinforcement or without transverse web reinforcement. In the parametric analysis, the quantities of the constitutive model parameter are identical to those in the benchmark analysis. In the case of Beam B1 ($a/d = 0.3$) (see Fig. 12), the longitudinal web reinforcement contributes significantly to the load-carrying capability, while the transverse web reinforcement does little. This may be explained by the fact that the inclination of the diagonal cracks is relatively close to the vertical direction (see Fig. 6a), and therefore the longitudinal web reinforcement restrains the crack opening displacement resulting in the small strength reduction of the compression strut between diagonal cracks. In the case of Beam B5 ($a/d = 1.9$) (see Fig. 13), the effect of the transverse web reinforcement increases and that of the longitudinal web reinforcement decreases. This may be explained by the fact that the cracking direction is inclined toward the horizontal direction (see Fig. 6b), and therefore the transverse web reinforcement also effectively restrains the crack opening.

Figures 14 and 15 show the effect of the maximum strength reduction rate c for the load-deflection relations in the parametric analyses without longitudinal web reinforcement or without transverse web reinforcement. In the parametric analyses, the quantities of the constitutive model parameters except c are identical to those in the benchmark analysis. The

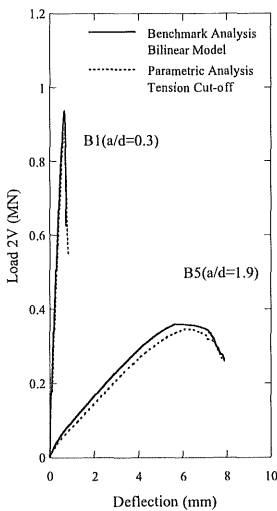


Figure 10. Comparison with Parametric Analysis in terms of f_{tu} .

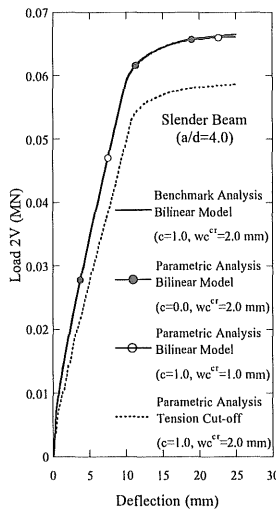


Figure 11. Comparison of Slender Beam in terms of c , w_c^{cr} and f_{tu} .

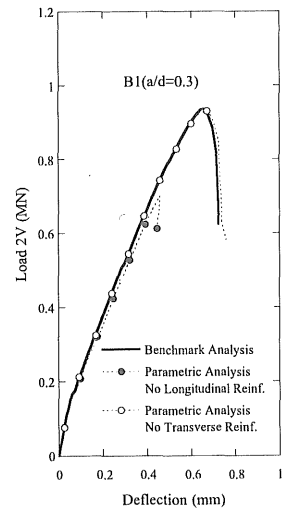


Figure 12. Comparison of Beam B1 without Web Reinforcement.

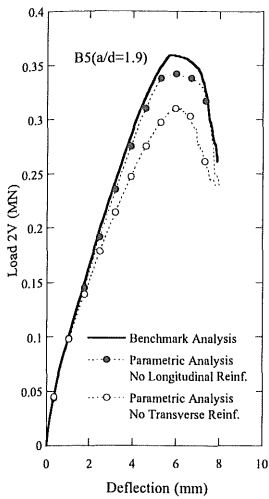


Figure 13. Comparison of Beam B5 without Web Reinforcement.

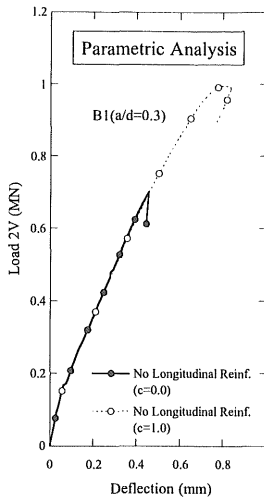


Figure 14. Comparison of Beam B1 without Web Reinf. in terms of c .

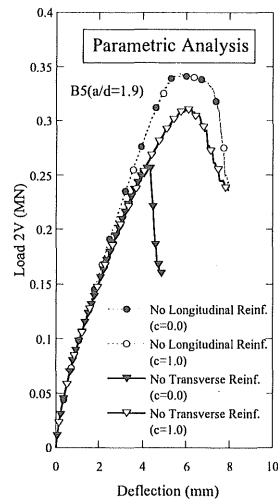


Figure 15. Comparison of Beam B5 without Web Reinf. in terms of c .

parametric analyses for Beam B1 ($a/d = 0.3$) without longitudinal web reinforcement gives larger difference between the numerical results with $c = 0.0$ and 1.0 (see Fig. 14) than the previous comparison (see Fig. 8). On the other hand, the parametric analyses for Beam B5 ($a/d = 1.9$) without longitudinal web reinforcement gives little difference between the numerical results with $c = 0.0$ and 1.0 (see Fig. 15), which is identical to the previous comparison (see Fig. 8). However, the parametric analyses for Beam B5 ($a/d = 1.9$) without transverse web reinforcement gives larger difference between the numerical results with $c = 0.0$ and 1.0 than the previous comparison (see Fig. 8). Thus, the longitudinal web reinforcement reduces the sensitivity of numerical simulation to the compressive strength reduction rate in the case of Beam B1 ($a/d = 0.3$), and the transverse web reinforcement reduces the sensitivity in the case of Beam B5 ($a/d = 1.9$).

4 CONCLUSIONS

In this paper, numerical simulations were carried out to examine the performance of constitutive models for describing the cracking behavior and the load-displacement characteristics of shear failure of fiber reinforced concrete structures. Based on the structural analysis for the shear-span ratio of 0.3 to 4.0, the following conclusions can be drawn.

The compressive strength reduction rate after cracking considerably influences the prediction of shear failure of concrete beams. Particularly, a large

compressive strength reduction rate is necessary to approximate the shear behavior of the beams with a small shear-span ($a/d = 0.3$). However, the sensitivity of the compressive strength reduction rate is reduced by the web reinforcement.

The compression-softening curve does not influence the entire load-deflection relation nor the peak load in the case of small shear-span ($a/d = 0.3$). However, in the case of large shear-span ($a/d = 1.9$), the post-peak ductility in the compressive constitutive law allows the increase of the shear load-carrying capability of beams. In the case of $a/d = 4.0$, the compression-softening curve does not influence the entire load-deflection relation nor the peak load since the flexural failure mode is dominant.

In the case of large shear-spans ($a/d = 1.9$ or higher), especially when the flexural failure mode is dominant, the post-peak ductility in the tensile constitutive law allows the increase of the shear load-carrying capability of beams

The longitudinal web reinforcement contributes to the shear load-carrying capability, while the transverse web reinforcement has little effect in the case of small shear-spans ($a/d = 0.3$). In the case of large shear-spans ($a/d = 1.9$), the effect of the transverse web reinforcement increases and that of the longitudinal web reinforcement decreases.

The longitudinal web reinforcement reduces the sensitivity of numerical simulation to the compressive strength reduction rate in the case of Beam B1 ($a/d = 0.3$), and the transverse web reinforcement reduces the sensitivity in the case of Beam B5 ($a/d = 1.9$).

REFERENCES

- American Concrete Institute 1989. *Building Code Requirements for Reinforced Concrete (ACI 318-89)*, American Concrete Inst., Detroit, Michigan.
- Bazant, Z.P. and Oh, B.H. 1983. Crack Band Theory for Fracture of Concrete, *Materials and Structures*, RILEM, Vol. 16, pp.155-177.
- CEB-FIP Model Code 90 1990. First Draft, Comite Euro-International du Beton, Bulletin d'information, No. 195,196, Mars.
- Chen, W.F. & Saleeb, A.F. 1982. *Constitutive Equations for Engineering Materials*, John Willey & Sons.
- Chen, W. F. 1982. *Plasticity in Reinforced Concrete*, McGraw-Hill Book Company.
- Hillerborg, A. & Rots, J. 1989. Crack Concepts and Numerical Modelling, in *Fracture Mechanics of Concrete Structures: from theory to applications*, (ed. L. Elfgren), CHAPMAN AND HALL, pp.128-146.
- Hordijk, D.A., Mier, J.G.M. van & Reinhardt, H.W. 1989. Material Properties in *Fracture Mechanics of Concrete Structures: from theory to applications*, (ed. L. Elfgren), CHAPMAN AND HALL, pp.67-127.
- Hordijk, D.A. 1991. *Local Approach to Fatigue of Concrete*, Doctoral Dissertation, Delft University of Technology, The Netherlands.
- Kollegger, J. - Mehlhorn, G. 1988. Experimentelle und Analytische Untersuchungen zur Aufstellung eines Materialmodells fuer Gerissene Stahbetonscheiben, Nr.6 Forschungsbericht, Massivbau, Gesamthochschule Kassel.
- Kupfer, H., Hilsdorf, H.K. & Rusch, H. 1969. Behavior of Concrete under Biaxial Stress, *ACI Journal*, V.66, No.8, Aug., pp.656-666.
- Lim, T. Y., Paramasivam, P., Mansur, M.A. & Lee, S. L. 1986. Tensile Behavior of Steel-Fiber Reinforced Cementitious Composites, *Proceedings, 3rd RILEM International Symposium on Developments in Fiber Reinforced Cement and Concrete*, University of Sheffield, pp. 7-16.
- Mansur, M.A. & Ong, K.C.G. 1991. Behavior of Reinforced Fiber Concrete Deep Beams in Shear, *ACI Struct. J.*, Vol. 88, No. 1, Jan.-Feb., pp. 98-105.
- Mier, J.G.M. van 1986. Multiaxial Strain-softening of Concrete, Part I: *fracture, Materials and Structures*, RILEM, Vol. 19, No.111.
- Rots, J. G. & Blaauwendraad, J. 1989. Crack Models for Concrete: Discrete or Smeared? Fixed, Multi-directional or Rotating?, *HERON*, Vol. 34, No. 1.
- SBETA 1997. *SBETA Computer program for nonlinear finite element analysis of reinforced concrete structures in plane stress state*, Program documentation, Cervenka Consulting, Prague.
- Vecchio F. J. & Collins M. P. 1986. The Modified Compression-field Theory for Reinforced Concrete Elements subjected to Shear, *ACI Journal* 83(2), pp. 219-231.